ELSEVIER

Two novel Mo(V) and Mo(V)/Mo(VI) barium phosphates with a tunnel structure: β-Ba(MoO)$_2$(P$_2$O$_7$)$_2$, and Ba(MoO)$_2$O(P$_2$O$_7$)PO$_4$

André Leclaire*, Valérie Pralong, Bernard Raveau

Laboratoire de Cristallographie et Sciences des Matériaux, Unité Mixte de Recherche 6508 du Centre National de la Recherche Scientifique, Ecole Nationale Superieure d'Ingénieurs de Caen et Centre de Recherche, Université de Caen, Ensicaen, Equipe de Cristallographie 6, Boulevard du maréchal Juin, FR-14050 Caen Cedex, France

Abstract

Two new Mo(V) and Mo(V)/Mo(VI) phosphates, β-Ba(MoO)$_2$(P$_2$O$_7$)$_2$ and Ba(MoO)$_2$O(P$_2$O$_7$)PO$_4$, with original tunnel structures have been synthesized. The first one crystallizes in the space group $P2_1/n$ with $a = 8.004$ Å, $b = 7.899$ Å, $c = 9.539$ Å, $\beta = 91.67°$, and the second one in the space group Cc with $a = 13.020$ Å, $b = 9.686$ Å, $c = 8.636$ Å, $\beta = 99.50°$. β-Ba(MoO)$_2$(P$_2$O$_7$)$_2$ shows close relationships with the α-form, i.e., it consists of similar MoP$_2$O$_{11}$ units sharing their apices and forming [MoP$_2$O$_{10}$]$_\infty$ chains. It differs from the latter by the configuration of the chains, so that one chain is linked to four other identical chains, instead of six chains in the α-form. Like the α-form, the β-form exhibits intersecting tunnels running along [010] and [011] direction where the Ba^{2+} cations sit. The 3D-framework of the second phosphate Ba(MoO)$_2$O(P$_2$O$_7$)PO$_4$, is built up of MoO$_6$ octahedra, P$_2$O$_7$ groups, and PO$_4$ tetrahedra, can be described by the assemblage of zig-zag [Mo$_2$P$_2$O$_{14}$]$_\infty$ chains through PO$_4$ tetrahedra, forming large tunnels running along $\vec{c}$, occupied by Ba^{2+} cations. In this framework one observes that adjacent tunnels communicate through large six-sided windows, showing the opened character of this structure. The magnetic behaviour of these phosphates is discussed with respect to the results previously obtained by Canadell et al. [Chem. Mater. 9 (1997) 68].
© 2005 Elsevier Inc. All rights reserved.

Keywords: Mo(V) phosphates; Barium molybdenum phosphates; Tunnel structure; Magnetic properties of Mo(V) compounds; Crystal structure of molybdenum phosphates

1. Introduction

The possibility to synthesize pentavalent molybdenum phosphates was shown for the first time by Kierkegard and Longo [1] for the compound MoPO$_5$. After this pioneering work, a huge number of Mo(V) phosphates containing univalent cations was discovered (see for a review Ref. [2]). Several of them were shown to exhibit a tunnel structure, allowing large cations like cesium [3,4] or potassium [5] to be hosted. In contrast, the number of Mo(V) phosphates containing large divalent cations like barium or strontium is rather limited. Beside the Mo(VI) barium phosphates Ba(MoO$_2$)$_2$(PO$_4$)$_2$ [6], only two

Mo(V) barium phosphates with a tunnel structure have been synthesized to date, the "mono-di" phosphate Li$_2$Ba$_{0.5}$(MoO)$_3$(PO$_4$)$_3$P$_2$O$_7$ [7] and the diphosphate Ba(MoO)$_2$(P$_2$O$_7$)$_2$ [8].

During the study of the last one we observed the existence of several other molybdenum phosphates whose structure could not be determined due to the too small size of the crystals. Moreover, all the syntheses of barium diphosphates led to mixtures. Bearing in mind that extra adducts, like lead chloride or bromide, are susceptible to stabilize new structures and allow their crystal growth, we have revisited the Mo(V)–Ba–P–O system, using PbBr$_2$ as adduct. We report herein on two novel Mo(V) phosphates, with original tunnel structures. The first one has the same composition as the Mo(V) barium diphosphate previously synthesized [8]

*Corresponding author. Fax: +33 2 31 95 16 00.

E-mail address: andre.leclaire@ensicaen.fr (A. Leclaire).

and will be labelled β-Ba(MoO)$_2$(P$_2$O$_7$)$_2$, whereas the second one Ba(MoO)$_2$O(P$_2$O$_7$)PO$_4$, exhibits the mixed valence Mo(V)/Mo(VI).

2. Synthesis and crystal growth

Single crystals of the two title compounds were grown from the same batch of nominal composition BaPbBr-Mo$_2$P$_3$O$_{15}$. First BaCO$_3$, H(NH$_4$)$_2$PO$_4$, and MoO$_3$ were mixed in an agate mortar in the molar ratio 2:6:3.667 and heated at 673 K in a platinum crucible to decompose the ammonium phosphate and the carbonate. In a second step the resulting mixture added to metallic molybdenum powder, PbO$_2$ and PbBr$_2$ (0.333:1:1), was crushed in an agate mortar and sealed in an evacuated silica ampoule, and then heated for one day at 873 K, cooled at 2 K per hour to 473 K, and finally quenched to room temperature.

From the resulting product several kinds of single crystals were extracted: blue crystals of α-Ba(MoO)$_2$(P$_2$O$_7$)$_2$ [8] already known, greenish yellow crystals of β-Ba(MoO)$_2$(P$_2$O$_7$)$_2$, and black crystals of Ba(MoO)$_2$O(P$_2$O$_7$)PO$_4$.

Attempts to obtain pure phases starting from the nominal compositions of the phases with the process described above lead for Ba(MoO)$_2$(P$_2$O$_7$)$_2$ to a mixture of the α and β types, and for Ba(MoO)$_2$O(P$_2$O$_7$)PO$_4$ to a dark powder containing about 90% of the latter.

3. Crystal structure determinations

Data of both compounds were recorded at room temperature on an Enraf-Nonius CAD-4 CCD diffractometer using MoKα radiation ($\lambda = 0.71073$ Å) isolated with a graphite monochromator. The absorption corrections were computed by the Gaussian method taking into consideration the shape and the size of the crystals. The complete data set was used to refine the respective cell parameters (Table 1).

For β-Ba(MoO)$_2$(P$_2$O$_7$)$_2$ the systematic absences $h + l = 2n + 1$ for $h0l$ and $k = 2n + 1$ for $0k0$, characteristic of the $P2_1/n$ space group, were observed. For Ba(MoO)$_2$O(P$_2$O$_7$)PO$_4$ the systematic absences $h + k = 2n + 1$ for all the hkl and $l = 2n + 1$ for $h0l$ were found to be consistent with the Cc and $C2/c$ space groups. The Patterson function showed many $0V\frac{1}{2}$ or $\frac{1}{2}V\frac{1}{2}$ Harker peaks and very few $U0W$ or $U\frac{1}{2}W$ Harker peaks indicating that the space group is rather Cc than $C2/c$. The refinements of the structure were successful with the non-centrosymmetric space group Cc.

Both structures were solved with the heavy atom method. The full-matrix least-squares refinements of the coordinates and of the anisotropic thermal motions of all atoms were performed on F weighted by $1/\sigma(F)^2$

Table 1
Summary of crystal data, intensity measurement, and structure refinement for β-Ba(MoO)$_2$(P$_2$O$_7$)$_2$ and Ba(MoO)$_2$O(P$_2$O$_7$)PO$_4$

	β-Ba(MoO)$_2$(P$_2$O$_7$)$_2$	Ba(MoO)$_2$O(P$_2$O$_7$)PO$_4$
Chemical formula	BaMo$_2$O$_{16}$P$_4$	BaMo$_2$O$_{14}$P$_3$
Space group	$P2_1/n$	Cc
a (Å)	8.0040(1)	13.0208(1)
b (Å)	7.8993(1)	9.6860(1)
c (Å)	9.5393(1)	8.6366(1)
β (deg)	91.673(3)	99.508(3)
V (Å^3)	602.87(3)	1075.1(1)
Z	2	4
Molecular weight	709.10D	646.13D
Density (g cm^{-3})	3.910	3.991
Linear absorption (mm^{-1})	5.916	6.450
T_{min}	0.7886	0.8379
T_{max}	0.8611	0.9297
Crystal size (mm)	0.036 × 0.042 × 0.050	0.012 × 0.028 × 0.028
Number of measurement	10763	8287
Number of $I \geqslant 3\sigma(I)$	10117	5511
Number of independent hkl with $I \geqslant 3\sigma(I)$	2854	3203
Extinction g_{iso}	0.08(2)	0.23(3)
Refined parameters	107	180
R (%)	3.39	4.37
R_w (%)	2.48	3.59
σ/Δ	0.0003	0.0002

with the JANA98 package [9]. They lead to $R = 0.0339$ and $R_w = 0.0248$ for β-Ba(MoO)$_2$(P$_2$O$_7$)$_2$ and to $R = 0.0437$ and $R_w = 0.0359$ for Ba(MoO)$_2$O(P$_2$O$_7$)PO$_4$, and to the atomic parameters of Table 2.

4. Description of the structures

4.1. The mixed valent Mo(V)/Mo(VI) phosphate Ba(MoO)$_2$O(P$_2$O$_7$)PO$_4$

The projection of the structure of this phosphate along $\vec{c}$ (Fig. 1) shows that it consists of a tridimensional framework [Mo$_2$P$_3$O$_{14}$]$_\infty$ built up of three sorts of units sharing their apices: PO$_4$ tetrahedra, diphosphate groups P$_2$O$_7$, and bioctahedral units Mo$_2$O$_{11}$. This host lattice forms large tunnels running along $\vec{c}$, and occupied by Ba^{2+} cations. One important feature of this structure deals with the existence of two free apices and one free apex for the P$_2$O$_7$ groups and the MoO$_6$ octahedra, respectively. Moreover, these free apices form the walls of the tunnels. In fact, the entire structure can be described by the assemblage of zig-zag chains [Mo$_2$P$_2$O$_{16}$]$_\infty$ running along $\vec{b}$, and of single monophosphate groups (Fig. 1). In each chain, the MoO$_6$ octahedra and the PO$_4$ tetrahedra share their apices in such a way that

Table 2
Atomic coordinates of β-Ba(MoO)$_2$(P$_2$O$_7$)$_2$ and Ba(MoO)$_2$O(P$_2$O$_7$) PO$_4$

Atom	x	y	y	U_{eq}	Site
Mo1	0.54575(3)	0.22337(3)	0.16170(2)	0.00598(5)	4e
Ba1	0.00000	0.00000	0.00000	0.00899(6)	2a
P1	0.17402(9)	0.39670(9)	0.21147(7)	0.0074(2)	4e
P2	0.27907(9)	0.40814(9)	−0.06724(7)	0.0066(2)	4e
O1	0.6984(3)	0.1246(3)	0.0801(2)	0.0162(6)	4e
O2	0.3970(3)	0.0265(2)	0.1877(2)	0.0116(5)	4e
O3	0.4128(3)	0.2867(3)	−0.0128(2)	0.0126(5)	4e
O4	0.6397(2)	0.1951(3)	0.3611(2)	0.0103(5)	4e
O5	0.6570(3)	0.4562(3)	0.1642(2)	0.0129(5)	4e
O6	0.3511(2)	0.3542(3)	0.2658(2)	0.0100(5)	4e
O7	0.2035(2)	0.5001(3)	0.0647(2)	0.0106(5)	4e
O8	0.0656(3)	0.2506(3)	0.1772(2)	0.0145(6)	4e
Ba1	0.50000	0.54835(5)	0.5000	0.0120(1)	4a
Mo1	0.34385(8)	0.14777(8)	0.6713(1)	0.0068(2)	4a
Mo2	0.15063(8)	0.66527(8)	0.3476(1)	0.0066(2)	4a
P1	0.2852(2)	0.3956(3)	0.1994(3)	0.0067(7)	4a
P2	0.2201(2)	0.1193(3)	0.3072(3)	0.0084(7)	4a
P3	0.0069(3)	0.5697(2)	0.0059(4)	0.0066(5)	4a
O1	0.3811(4)	0.3028(7)	0.6117(7)	0.014(5)	4a
O2	0.2331(4)	0.2033(6)	0.7705(7)	0.011(2)	4a
O3	0.2368(5)	0.1070(7)	0.4901(8)	0.012(2)	4a
O4	0.4490(4)	0.0452(7)	0.5735(7)	0.014(2)	4a
O5	0.4367(6)	0.1617(7)	0.8844(9)	0.009(2)	4a
O6	0.3089(4)	−0.0555(6)	0.7369(7)	0.011(2)	4a
O7	0.0796(4)	0.7764(6)	0.4386(7)	0.013(2)	4a
O8	0.0899(4)	0.4952(6)	0.4208(7)	0.011(2)	4a
O9	0.2731(5)	0.6379(7)	0.5251(8)	0.011(2)	4a
O10	0.0517(6)	0.6712(7)	0.1352(9)	0.013(2)	4a
O11	0.2289(4)	0.5268(6)	0.2272(7)	0.012(2)	4a
O12	0.2254(5)	0.2808(6)	0.2806(8)	0.018(2)	4a
O13	0.3992(5)	0.4011(8)	0.2615(9)	0.015(2)	4a
O14	0.1116(5)	0.0728(7)	0.2432(9)	0.013(2)	4a

Fig. 1. Projection of the structure of Ba(MoO)$_2$O(P$_2$O$_7$)PO$_4$ along $\vec{c}$. The view is in fact tilted by about 2° with respect to the $\vec{c}$ direction in order to better identify the [Mo$_2$P$_2$O$_{16}$]$_\infty$ chains (in bold drawing).

one P$_2$O$_7$ group alternates with one bioctahedral unit. In the (100) plane, two successive [Mo$_2$P$_2$O$_{16}$]$_\infty$ chains share the apices of their polyhedra so that each P$_2$O$_7$ group of one chain is linked to each Mo$_2$O$_{11}$ group of the adjacent chain forming [Mo$_2$P$_2$O$_{14}$]$_\infty$ layers parallel to (1 0 0). As a consequence, the 3D framework [Mo$_2$P$_3$O$_{14}$]$_\infty$ consists of [Mo$_2$P$_2$O$_{14}$]$_\infty$ layers of dimeric units P$_2$O$_7$ and Mo$_2$O$_{11}$ interconnected by layers of isolated PO$_4$ tetrahedra (Fig. 1). Note that in these (100) layers the P$_2$O$_7$ groups and Mo$_2$O$_{11}$ bioctahedra form rather large six sided windows, which ensure the communication between two adjacent tunnels. The opened character of this structure can also be evidenced by describing the [Mo$_2$P$_3$O$_{14}$]$_\infty$ frameworks as the stacking of [Mo$_2$P$_3$O$_{18}$]$_\infty$ layers either along [101] or along $\vec{c}$. In both cases one recognizes the [Mo$_2$P$_2$O$_{16}$]$_\infty$ chains running along $\vec{b}$, interconnected though single PO$_4$ tetrahedra. But more importantly, these (101) and (001) layers exhibit large windows, the barium cation sitting in the larger ones, i.e., at the level of the (101) layers. Finally, it is worth pointing out that in the (001)
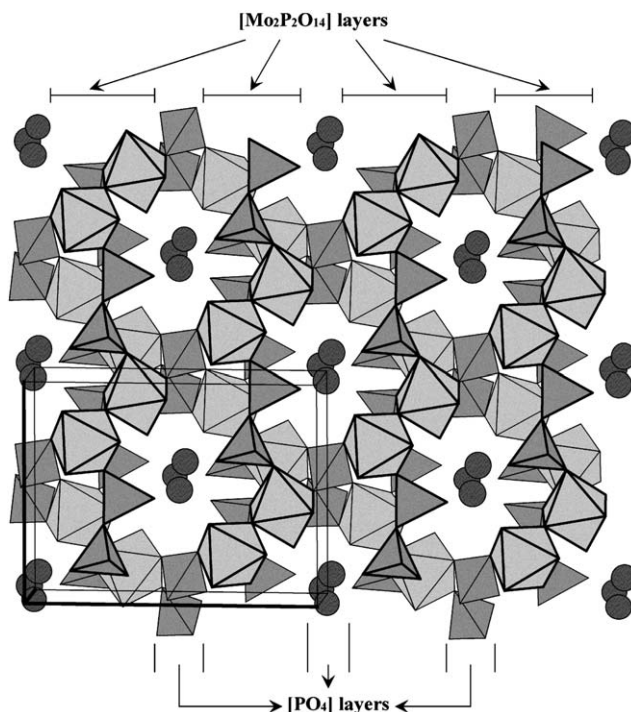
layer the "Mo$_2$O$_{11}$" bioctahedra and the single PO$_4$ tetrahedra share apices forming [Mo$_2$PO$_{13}$]$_\infty$ chains running along [110], so that these [Mo$_2$P$_3$O$_{18}$]$_\infty$ layers can also be described as the assemblage of these chains through the P$_2$O$_7$ groups.

The geometry of the PO$_4$ tetrahedra is in agreement with that usually observed, covering a rather wide range of P–O bond lengths (Table 3), due to the diversity of bonding modes. The longest P–O bonds (1.584–1.586 Å) correspond to the bridging oxygen atom between the P(1) and the P(2) tetrahedra in the P$_2$O$_7$ group, whereas the shorter ones (1.495–1.500 Å) are observed for the free apices of the P(1) and the P(2) tetrahedra. The distances corresponding to the P–O–Mo bonds are intermediate, ranging from 1.506 to 1.563 Å.

The geometry of the MoO$_6$ octahedra forming the Mo$_2$O$_{11}$ bioctahedral units is in favour of an electronic delocalisation between the two octahedra Mo(1) and Mo(2). One indeed observes an average Mo–O distance of 1.943 Å for Mo(1) and of 1.949 Å for Mo(2), showing the absence of charge ordering. This view point is supported by the bond valence sums calculated with the universal constant determined by Zocchi [10] for molybdenum. One observes formal charges of 5.42 and 5.31 for Mo(1) and Mo(2), respectively, in agreement with the average value 5.50 deduced from the chemical formula. Like for the Mo(V) octahedra, each mixed valent Mo(V)–Mo(VI) octahedron exhibits one very short bond (1.68–1.695 Å) corresponding to its free

Table 3
Distances (Å) and angles (deg) in $Ba(MoO)_2O(P_2O_7)PO_4$

Mo1	O1	O2	O3	O4	O5	O6
O1	**1.685(7)**	2.722(9)	2.854(9)	2.696(9)	2.716(10)	3.799(9)
O2	99.6(3)	**1.876(6)**	2.603(9)	3.840(8)	2.704(9)	2.728(8)
O3	98.0(3)	85.5(3)	**1.957(6)**	2.804(8)	3.966(9)	2.691(9)
O4	93.6(3)	166.7(3)	90.6(3)	**1.990(6)**	2.941(10)	2.670(9)
O5	93.4(3)	87.5(3)	167.5(3)	93.9(3)	**2.033(7)**	2.850(9)
O6	174.5(3)	85.9(2)	82.5(2)	81.0(3)	86.7(2)	**2.119(6)**

Mo2	O2^i	O7	O8	O9	O10	O11
O2^i	**1.858(6)**	2.665(8)	3.807(8)	2.664(9)	2.741(9)	2.640(8)
O7	97.1(3)	**1.695(6)**	2.733(9)	2.845(8)	2.779(10)	3.760(9)
O8	166.3(2)	95.9(3)	**1.976(6)**	2.777(8)	2.972(9)	2.678(9)
O9	86.1(3)	98.8(3)	87.5(2)	**2.039(6)**	4.069(9)	2.760(9)
O10	88.6(3)	94.9(3)	94.8(3)	165.8(3)	**2.061(7)**	2.704(9)
O11	84.4(3)	176.5(2)	82.9(2)	84.5(2)	81.9(3)	**2.067(6)**

P1	O9^i	O11	O12	O13
O9^i	**1.522(7)**	2.501(9)	2.516(10)	2.430(9)
O11	111.3(4)	**1.506(6)**	2.429(8)	2.506(9)
O12	108.0(4)	103.5(4)	**1.586(7)**	2.576(10)
O13	107.3(4)	113.2(4)	113.5(4)	**1.495(7)**

P2	O3	O6^{ii}	O12	O14
O3	**1.563(7)**	2.568(10)	2.458(9)	2.484(9)
O6^{ii}	112.6(4)	**1.524(6)**	2.496(8)	2.586(9)
O12	102.7(4)	106.8(4)	**1.584(7)**	2.491(9)
O14	108.4(4)	117.6(4)	107.7(4)	**1.500(7)**

P3	O4^{iii}	O5^{iv}	O8^i	O10
O4^{iii}	**1.515(7)**	2.573(10)	2.479(8)	2.497(9)
O5^{iv}	114.0(4)	**1.554(8)**	2.487(9)	2.424(10)
O8^i	108.5(3)	107.1(4)	**1.539(7)**	2.565(10)
O10	110.2(4)	103.6(4)	113.4(4)	**1.529(8)**

Ba–O distances (Å) in the coordination polyhedra
Ba1–O14^v	2.626(7)
Ba1–O13	2.666(7)
Ba1–O13^{vi}	2.836(8)
Ba1–O14^{vii}	2.856(8)
Ba1–O7^{viii}	2.912(7)
Ba1–O10^{ix}	2.989(7)
Ba1–O5^i	3.048(7)
Ba1–O1	3.079(6)
Ba1–O9	3.123(7)
Ba1–O3^{vii}	3.153(7)

The Mo–O or P–O distances are in bold on the diagonal, the O–O distances are above it and the O–Mo–O or O–P–O are under it.
Symmetry codes: i: x; $1-y$; $z-\frac{1}{2}$; ii: x; $-y$; $z-\frac{1}{2}$; iii: $x-\frac{1}{2}$; $\frac{1}{2}-y$; $z-\frac{1}{2}$; iv: $x-\frac{1}{2}$; $\frac{1}{2}+y$; $z-1$, v: $\frac{1}{2}+x$; $\frac{1}{2}-y$; $\frac{1}{2}+z$, vi: x; $1-y$; $\frac{1}{2}+z$, vii: $\frac{1}{2}+x$; $\frac{1}{2}+y$; z, viii: $\frac{1}{2}+x$; $y-\frac{1}{2}$; z, viii: $\frac{1}{2}+x$; $3/2-y$; $\frac{1}{2}+z$.

apex, opposed to an abnormally long one (2.119–2.067 Å), whereas the four other equatorial bonds are intermediate (Table 3). However, it must be emphasized that owing to the latter, the Mo–O distances corresponding to the bridging oxygen between the two Mo(1) and Mo(2) octahedra are significantly smaller

(1.858–1.876 Å) than the three others (1.955 → 2.067 Å). Such a feature is also in agreement with the possible delocalisation of the electron between the two adjacent Mo(1) and Mo(2) species.

The barium cations are surrounded by ten oxygen atoms forming distorted bicapped antiprisms with Ba–O distances ranging from 2.626 to 3.153 Å (Table 3).

4.2. The Mo(V) diphosphate β-Ba(MoO)$_2$(P$_2$O$_7$)$_2$

The diphosphate β-Ba(MoO)$_2$(P$_2$O$_7$)$_2$ exhibits, like the α-form previously evidenced [8], a tridimensional framework built up of corner sharing MoO$_6$ octahedra and P$_2$O$_7$ groups. The projection of the structure of this disphosphate along $\vec{b}$ (Fig. 2a) compared to that of the α-form along $\vec{a}$ (Fig. 2b) shows the close relationships between the two [Mo$_2$P$_2$O$_{16}$]$_\infty$ frameworks.

Both structures exhibit identical MoP$_2$O$_{11}$ units (inset Fig. 2a) built up of one P$_2$O$_7$ group sharing two apices with the same octahedra. In the two form the entire framework can be described by the association of these MoP$_2$O$_{11}$ units through their corners. Thus, in the two structures, the MoP$_2$O$_{11}$ units share their apices forming infinite [MoP$_2$O$_{10}$]$_\infty$ chains, where one P$_2$O$_7$ group alternates with one MoO$_6$ octahedron. These chains run along [101] and along $\vec{b}$ for the β and α forms, respectively (Fig. 2). However, the configuration of the [MoP$_2$O$_{10}$]$_\infty$ chains is different in the two structures. In the β-form, the P$_2$O$_7$ groups sit on the same side of the axis of the [MoP$_2$O$_{10}$]$_\infty$ chain adopting a left (or right) hand configuration as shown for the (010) layers of this disphosphate (inset Fig. 2a), whereas in the α-form the P$_2$O$_7$ groups sit on each side of the axis of the chain alternately, adopting a mixed right–left hand configuration as shown for the (001) layers of this form (inset Fig. 2b). As a consequence, the assemblage of the [MoP$_2$O$_{10}$]$_\infty$ chains is different in the two structures: one [MoP$_2$O$_{10}$]$_\infty$ chain is linked to identical four chains in the β Ba(MoO)$_2$(P$_2$O$_7$)$_2$ structure, whereas one observes that one [MoP$_2$O$_{10}$]$_\infty$ chain is linked to six identical chains in the α-form.

It results that the nature of the tunnels formed by the host lattice is different in these structures, as illustrated in Fig. 2 for the tunnels running along $\vec{b}$ and $\vec{a}$ for the β and α form, respectively. Moreover, it is remarkable that both disphosphates exhibit intersecting tunnel structures. In the β-form, one indeed observes that besides the [010] tunnels (Fig. 2a), there exist tunnels running along [100] (Fig. 3a) and that the Ba^{2+} cations sit at the intersection of these tunnels. Similarly, α-Ba(MoO)$_2$(P$_2$O$_7$)$_2$ also shows [001] tunnels (Fig. 3b) which intersect with the [100] tunnels (Fig. 2b), with Ba^{2+} cations located at the intersection.

The geometry of the MoO$_6$ octahedra in this new β-form is very similar to that observed for the α-one, and characteristic of pentavalent molybdenum. One
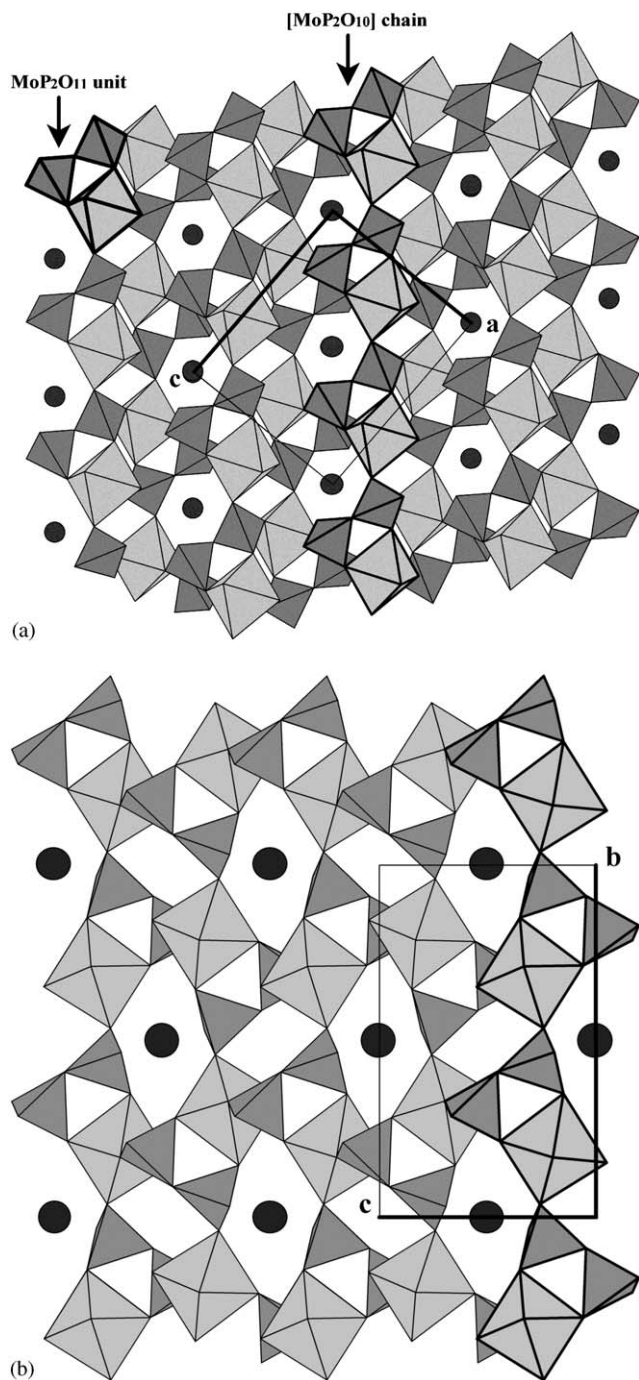
Fig. 2. (a) The β-Ba(MoO)$_2$(P$_2$O$_7$)$_2$ frameworks projected along $\vec{b}$. One MoP$_2$O$_{11}$ "cat head" unit is drawn in hard bold and one [MoP$_2$O$_{10}$]$_\infty$ chain running along [101] is drawn in bold. (b) The α-Ba(MoO)$_2$(P$_2$O$_7$)$_2$ frameworks projected along $\vec{a}$ with the [MoP$_2$O$_{10}$]$_\infty$ chain (in bold) running along $\vec{b}$.

Fig. 3. (a) Projection of the structure of β-Ba(MoO)$_2$(P$_2$O$_7$)$_2$ along $\vec{a}$ showing the tunnels. (b) Projection of the structure of α-Ba(MoO)$_2$ (P$_2$O$_7$)$_2$ along $\vec{c}$ showing the existence of tunnels along this direction.

observes Mo^{5+} with one very short molybdenyl bond (1.662 Å) opposed to a long one (2.138 Å) and four intermediate Mo–O bonds (1.977 $\rightarrow$ 2.041 Å) (Table 4). The P–O bond lengths are correlated to the number and to the size of the bonds shared with the other atoms. When the oxygen atom bridges the two phosphorus of the disphosphate group, the P–O distances are very long (1.588–1.643 Å). For the "free corner", the P–O distance is short (1.474 Å), the other ones ranging from 1.513 to 1.532 Å according to the coordination of the oxygen atoms. The bond valence sums determined with the Brese and O'Keeffe formulation [11] using a more appropriate R_{ij} value for Molybdenum [12] are in agreement with the theoretical charges deduced from the chemical formula.

The Ba^{2+} cation is surrounded by ten oxygen atoms with Ba–O distances ranging from 2.664 to 3.492 Å, delimiting a bicapped cube less distorted than that observed in the α-form.

5. Discussion and conclusions

Bearing in mind the structural classification proposed previously for the Mo(V) and Mo(V)–Mo(VI) phosphates [2], based on the number of octahedra sharing corners and edges in the "Mo(V)–P–O" framework, one

Table 4
Distances (Å) and angles (deg) in β-Ba(MoO)$_2$(P$_2$O$_7$)$_2$

Mo1	O1	O2	O3	O4	O5	O6
O1	**1.662(2)**	2.760(3)	2.744(3)	2.791(3)	2.759(3)	3.799(3)
O2	98.3(1)	**1.977(2)**	2.811(3)	2.845(3)	3.988(3)	2.718(3)
O3	96.2(1)	89.60(9)	**2.012(2)**	4.020(3)	2.875(3)	2.769(3)
O4	97.45(9)	90.23(8)	166.28(9)	**2.037(2)**	2.794(3)	2.760(3)
O5	95.8(1)	165.84(9)	90.36(9)	86.48(8)	**2.041(2)**	2.779(3)
O6	179.1(1)	82.61(8)	83.65(8)	82.72(7)	83.32(9)	**2.138(2)**

P1	O2^i		O6		O7		O8
O2^i	**1.526(2)**		2.458(3)		2.526(3)		2.543(3)
O6	107.0(1)		**1.532(2)**		2.504(3)		2.548(3)
O7	105.6(1)		104.0(1)		**1.643(2)**		2.513(3)
O8	115.9(1)		115.9(1)		107.3(1)		**1.474(2)**

P2	O3		O4^{ii}		O5^{iii}		O7
O3	**1.517(2)**		2.468(3)		2.543(3)		2.502(3)
O4^{ii}	108.4(1)		**1.527(2)**		2.506(3)		2.519(3)
O5^{iii}	114.1(1)		111.1(1)		**1.513(2)**		2.505(3)
O7	107.4(1)		108.0(1)		107.7(1)		**1.588(2)**

Ba1–O8	2.644(2)
Ba1–O8^{iv}	2.644(2)
Ba1–O1^v	2.736(2)
Ba1–O1vi	2.736(2)
Ba1–O6^{vii}	2.753(2)
Ba1–O6^{ii}	2.753(2)
Ba1–O4^{vii}	2.980(2)
Ba1–O4^{ii}	2.980(2)
Ba1–O5^{vii}	3.492(2)
Ba1–O5^{ii}	3.492(2)

The Mo–O or P–O distances are in bold on the diagonal, the O–O distances are above it and the O–Mo–O or O–P–O are under it.
Symmetry codes: i: $\frac{1}{2}-x$; $\frac{1}{2}+y$; $\frac{1}{2}-z$, ii: $x-\frac{1}{2}$; $\frac{1}{2}-y$; $z-\frac{1}{2}$, iii: $1-x$; $1-y$; $-z$, iv: $-x$; $-y$; $-z$, v: $x-1$; $-y$; $-z$, vi: $1-x$; $-y$; $-z$, vii: $\frac{1}{2}-x$; $y-\frac{1}{2}$; $\frac{1}{2}-z$.

observes that α and β Ba(MoO)$_2$(P$_2$O$_7$)$_2$ both belong to the class I, i.e., involve only isolated MoO$_6$ octahedra, whereas Ba(MoO)$_2$O(P$_2$O$_7$)PO$_4$ belongs to the class III, i.e., contains only bioctahedral "Mo$_2$O$_{11}$" units, built of two corner-shared octahedra. These structural features are of importance since it has been demonstrated by Canadell et al. [13] that the magnetic properties of these Mo(V) or Mo(V)–Mo(VI) phosphates are closely related to the nature of their octahedral units and especially to the number of octahedra that form such units and to their internal geometry indirectly influenced by the PO$_4$ tetrahedra.

The α and β-Ba(MoO)$_2$(P$_2$O$_7$)$_2$ diphosphates exhibit the structural behaviour, often observed in pure diphosphates belonging the class I, i.e., each isolated octahedron shares two corners with the same diphosphate group, forming the "MoP$_2$O$_{11}$" units described above. In this respect, it would be interesting to compare their magnetic behaviour with those previously observed for CsMoOP$_2$O$_7$ and KMoOP$_2$O$_7$ [13] which contain the

same "MoP$_2$O$_{11}$" structural units. Such a comparison would be more interesting because besides the antiferromagnetic behaviour observed for KMoOP$_2$O$_7$ ($T_N \approx 25$ K), and its normal C_M parameter which leads to 1.73 μ_B per Mo in agreement with the theoretical value for a spin only contribution, the diphosphate CsMoOP$_2$O$_7$ shows a much smaller value of 1.30 μ_B per Mo, which is to date unexplained. Unfortunately, the α- and β-Ba(Mo^{V}O)$_2$(P$_2$O$_7$)$_2$, cannot be separated in the polycrystalline sample. Nevertheless, we have carried out magnetic measurements versus temperature on this sample, considering that at high temperature, in the paramagnetic state the behaviour should be the same due to the presence of only Mo(V). The sample was first zero-field cooled down to 4.2 K and the magnetic moment was measured at increasing temperature from 4.2 to 300 K with a SQUID magnetometer in a magnetic field of 3000 Oe. The susceptibility curve $\chi(T)$ (Fig. 4a) shows a paramagnetic behaviour above 130 K; the data least squares fitted to a Curie–Weiss law, yield $\theta p = -115(5)$ K and an effective moment μ_{eff} per Mo(V) of
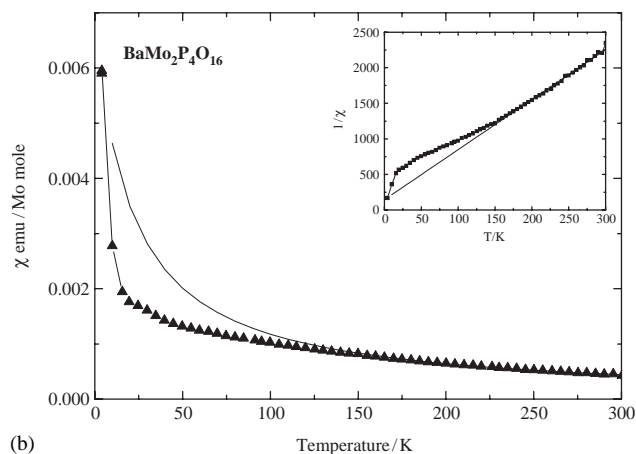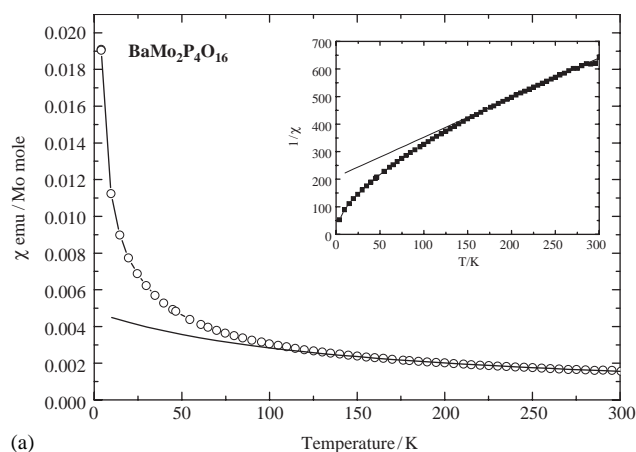

Fig. 4. The magnetic susceptibility χ versus temperature T of: (a) The powder mixture of α and β-Ba(MoO)$_2$(P$_2$O$_7$)$_2$, and (b) Ba(MoO)$_2$O (P$_2$O$_7$)PO$_4$.

1.18μ_B. The negative θp value suggests antiferromagnetic coupling at low temperature. The value of the magnetic moment, lower than that of $KMoOP_2O_7$ and $CsMoOP_2O_7$, suggests that the latter is greatly influenced by the nature of the lattice, but no further conclusion can be drawn from this measurement due to the fact that the two forms are present in the sample.

The phosphate $Ba(MoO)_2O(P_2O_7)PO_4$ is of great interest for two reasons. From the structural viewpoint, this compound is the first mixed valent "Mo(V)–Mo(VI)" phosphate whose framework contains simultaneously "Mo_2O_{11}" and P_2O_7 dimeric units. The association of disphosphate groups and bioctahedral "Mo_2O_{11}" units is indeed rather rare in molybdenum phosphates. It has been observed, to our knowledge, in three compounds only: the Mo(IV) phosphates $TlMo_2OP_2O_7$ PO_4 [14] and $Pb_2Mo_2O(PO_4)_2P_2O_7$ [15], and the Mo(III)–Mo(IV) phosphate $Cs_4Mo_6O_2(PO_4)_2$ $(P_2O_7)_4$ [16]. The arrangement of the Mo_2O_{11} and P_2O_7 units in this Mo(V)–Mo(VI) phosphate is also very different from that observed in the three other Mo(IV) and Mo(III)–Mo(IV) phosphates due to the existence of the molybdenyl Mo–O bonds in the Mo_2O_{11} octahedra. In $Ba(MoO)_2(P_2O_7)PO_4$, each P_2O_7 group shares only one apex with the same "Mo_2O_{11}" octahedral unit (Fig. 1), whereas in the Mo(IV) and Mo(III)–Mo(IV) phosphates each P_2O_7 group shares two apices with the same bioctahedral "Mo_2O_{11}" unit: one P_2O_7 group shares two apices with two different octahedra of the

Mo_2O_{11} unit in $TlMo_2OP_2O_7$ PO_4 (Fig. 5a) and in $Pb_2Mo_2O(PO_4)_2P_2O_7$ (Fig. 5b), or two apices with the same octahedron of the Mo_2O_{11} unit in $Cs_4Mo_6O_2$ $(PO_4)_2(P_2O_7)_4$ (Fig. 5c) [11]. From the physical viewpoint, the magnetic behaviour previously observed for the Mo(V)–Mo(VI) monophosphate and $Rb_3Mo_4O_6$ $(PO_4)_4$, which contains Mo_2O_{11} units, should also be compared to that in $Ba(MoO)_2O(P_2O_7)PO_4$. Canadell et al. [13] observed for the latter a magnetic moment of $0.5\,\mu_B$ per Mo(V) instead of $1.73\,\mu_B$ for the theoretical value. The probable existence of electronic delocalisation between the two Mo(1) and Mo(2) sites of the Mo_2O_{11} units in the $Ba(MoO)_2O(P_2O_7)PO_4$ phosphate, should also confer original magnetic properties to this compound. Unfortunately, the presence of a secondary phase beside this phosphate does not allow a rigorous study to be carried out. Nevertheless the magnetic measurements, carried out with a SQUID in the same conditions as described above, show a very different behaviour. A Curie–Weiss law is also observed above 150 K (Fig. 4b). The data, least-squares fitted with this law lead to $\theta p = -22$ K indicating an antiferromagnetic coupling at low temperature. More importantly, the deduced magnetic moment of $1.06\,\mu_B$ per Mo(V) is much smaller than the theoretical value ($1.73\,\mu_B$) in agreement with the probable electronic delocalisation between the two Mo(1) and Mo(2) sites, but remains much larger than that observed for $Rb_3(MoO)_2O$ $(P_2O_7)PO_4$. The presence of a secondary phase does not allow any further conclusion and it may be at the origin of the upturn of the susceptibility below 10 K.

In conclusion, two new barium phosphates containing Mo(V) with original tunnel structures have been synthesized, showing the great adaptability of the diphosphate groups either to single Mo(V) octahedra or two Mo(V)/Mo(VI) bioctahedral units. This study suggests that besides the huge number of molybdenum phosphates actually known, many others remain to be discovered, using adducts or soft chemistry methods. The magnetic properties of these materials, though they appear promising will require further investigation to obtain pure phases.

Fig. 5. Modes of connection of Mo_2O_{11} and P_2O_7 dimeric units in: (a) $TlMo_2O(P_2O_7)PO_4$, (b) $Pb_2Mo_2O(PO_4)_2(P_2O_7)$, and (c) $Cs_4Mo_6O_2$ $(PO_4)_2(P_2O_7)$.

References

[1] P. Kierkegaard, J.M. Longo, Acta Chem. Scand. 24 (1970) 427–432.

[2] G. Costentin, A. Leclaire, M.M. Borel, A. Grandin, B. Raveau, Rev. Inorg. Chem. 13 (1993) 77–101.

[3] K.H. Lii, C.C. Wang, J. Solid State Chem. 77 (1988) 117–123.

[4] R.C. Haushalter, F.W. Lai, J. Solid State Chem. 76 (1988) 218–223.

[5] A. Guesdon, A. Leclaire, M.M. Borel, A. Grandin, B. Raveau, J. Solid State Chem. 114 (1995) 481–485.

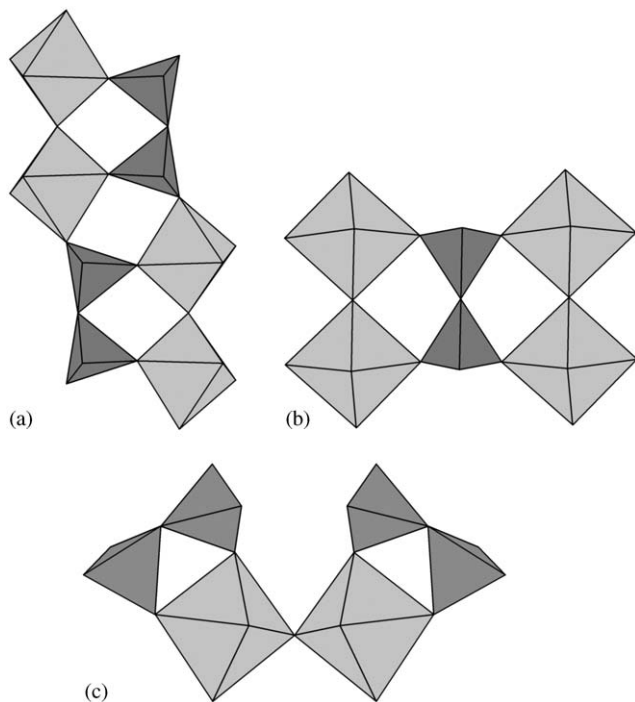[6] R. Masse, M.T. Averbuch-Pouchot, A. Durif, J. Solid State Chem. 58 (1985) 157–163.

[7] S. Ledain, A. Leclaire, M.M. Borel, M. Hervieu, J. Provost, B. Raveau, J. Solid State Chem. 144 (1999) 297–310.

[8] G. Costentin, M.M. Borel, A. Grandin, A. Leclaire, B. Raveau, J. Solid State Chem. 89 (1990) 83–87.

[9] V. Petricek, M. Dusek, JANA 98, Institute of Physics, Academy of Sciences of Czech Republic, 1998.

[10] F. Zocchi, J. Solid State Sci. 3 (2001) 383–386.

[11] N.E. Brese, M. O'Keeffe, Acta Crystallogr. B 47 (1991) 192–197.

[12] M.M. Borel, A. Leclaire, J. Chardon, J. Provost, B. Raveau, J. Solid State Chem. 141 (1998) 587–593.

[13] E. Canadell, J. Provost, A. Guesdon, M.M. Borel, A. Leclaire, Chem. Mater. 9 (1997) 68–75.

[14] A. Leclaire, J.C. Monier, B. Raveau, J. Solid State Chem. 59 (1985) 301–305.

[15] A. Leclaire, J. Chardon, B. Raveau, J. Solid State Chem. 172 (2003) 412–416.

[16] R.C. Haushalter, J. Solid State Chem. 89 (1990) 215–219.